Vegetation greenness and land carbon flux anomalies associated with climate variations with a focus on the year 2015

Chao Yue[1], Philippe Ciais[1], Ana Bastos[1], Frederic Chevallier[1], Yi Yin[1], Christian Rödenbeck[2], Taejin Park[3]

[1]Laboratoire des Sciences du Climat et de l'Environnement, CEA-CNRS-UVSQ, UMR8212, Gif-sur-Yvette, France

[2] Max Planck Institute for Biogeochemistry, Jena, Germany.

[3]Department of Earth and Environment, Boston University, Boston, MA 02215, USA

Corresponding author: Chao Yue, chao.yue@lsce.ipsl.fr

Abstract

Enhanced vegetation greening during the past decades over the northern hemisphere was found to be linked with an increasing land sink. In the meantime, interannual variability in the atmospheric CO_2 growth rate is strongly coupled with land carbon uptake dynamics in the tropics, driven by the El Niño–Southern Oscillation (ENSO) climate variations. One may thus wonder how land ecosystems respond to the co-occurrence of extreme greening and an El Niño event. The year 2015 provided an ideal case study for such examination. It was the greenest year since 2000 according to satellite observations of vegetation greenness, but a record atmospheric CO_2 growth rate also happened, associated with a weaker than usual land carbon sink. To reconcile these two observations that may seem paradoxical at first sight, we examined the patterns of large-scale CO_2 fluxes using two atmospheric inversions and the general links among vegetation greenness, seasonal land carbon uptake and climate variations. Inversion results indicate that the year 2015 had a higher than usual northern land carbon uptake in spring and summer, consistent with the greening anomaly. This higher uptake was however followed by a larger source of CO_2 in autumn, suggesting that the extra uptake during the growing season was coupled to and offset by a larger release in the late growing season. Vegetation greenness shows strong positive correlation with land carbon uptake in the northern hemisphere during the

growing season, but outside growing season their relation is rather weak. For the tropics and Southern Hemisphere, a strong and abrupt transition toward a large carbon source for the last trimester of 2015 is discovered, concomitant with the El Niño development. This transition of terrestrial tropical CO_2 fluxes between two consecutive seasons is the largest ever found in the inversion records. Although such strong transition to carbon source is consistent with historical observation of a strong dependence of land carbon uptake on tropical temperature and dryness, the detailed underlying mechanisms remain to be elucidated.

1 Introduction

The first monitoring station for background atmospheric CO_2 concentration was established at Mauna Loa in 1958. Its record shows that atmospheric CO_2 has continued to rise in response to anthropogenic emissions. However, the atmospheric CO_2 growth rate (AGR) has been lower than that implied by anthropogenic emissions alone, because land ecosystems and the oceans have absorbed part of the emitted CO_2 (Canadell et al., 2007; Le Quéré et al., 2016). Although on multi-decadal time scale carbon uptake by land and ocean has kept pace with growing carbon emissions (Ballantyne et al., 2012; Li et al., 2016), large year-to-year fluctuations occur in the terrestrial carbon sink, mainly in response to climate variations induced by El Niño–Southern Oscillation (ENSO) (Wang et al., 2013, 2014) and other occasional events such as volcanic eruptions (Gu et al., 2003). In northern latitude regions, increasing seasonal amplitude of atmospheric CO_2 is found to be linked with an increased land sink, associated with vegetation greening driven partly by long-term warming and CO_2 fertilization (Forkel et al., 2016; Graven et al., 2013; Myneni et al., 1997). The interannual variations in vegetation activity in the northern hemisphere are found to be mainly driven by temperature variations (Piao et al., 2014).

In 2015, the global monthly atmospheric CO_2 concentration surpassed 400 $\mu mol \cdot mol^{-1}$ (ppm) for the first time since the start of background measurements, with an unprecedented large annual growth rate of 2.96±0.09 ppm yr^{-1} (https://www.esrl.noaa.gov/gmd/ccgg/trends/global.html#global_growth). This record-breaking AGR occurred simultaneously with a high value of the ENSO index (Betts et al., 2016) and the warmest land temperature on record since 1880 (https://www.ncdc.noaa.gov/cag/time-

series/global/globe/land/ytd/12/1880-2015). At the same time, 2015 was also shown to have the greenest growing season of the Northern Hemisphere since 2000 (Bastos et al., 2017). Widespread abnormally high positive anomalies of the normalized difference vegetation index (NDVI) were observed from Moderate-resolution imaging spectroradiometer (MODIS) sensor aboard the Terra satellite, in particular over eastern North America and large parts of Siberia. On the one hand, strong greening is expected to enhance northern land carbon uptake during the growing season (Myneni et al., 1997); on the other hand, the strong El Niño event in the second half of 2015 increased fire emissions in tropical Asia (Huijnen et al., 2016; Yin et al., 2016) and likely caused a loss of plant biomass and reduced carbon uptake, possibly associated with the prevailing high temperatures and reduced rainfall (Ahlström et al., 2015; Jiménez-Muñoz et al., 2016).

To reconcile the observed maximum global land greening with the record-high AGR in 2015, we examined land-atmosphere carbon fluxes estimated from two atmospheric inversions. We examine the relationship between land carbon uptake anomalies and NDVI anomalies and climate anomalies, with a special focus on seasonal patterns in the land carbon uptake in 2015 relative to the long-term trend of 1981-2015. The aim here is to infer general patterns in factors driving the land carbon uptake anomalies and to examine how the carbon dynamics in 2015 fit into this pattern. We then focus how land ecosystems responded to the joint occurrences of record-breaking warming, extreme greening, and the end-of-year El Niño event, to understand how land ecosystems contributed to the high AGR in 2015.

2 Data and methods

2.1 Data sets

2.1.1 Atmospheric inversion data

We used two gridded land and ocean carbon uptake data sets based on atmospheric CO_2 observations, namely those from the Copernicus Atmosphere Monitoring Service (CAMS) inversion system developed at LSCE (Chevallier et al., 2005, 2010) and from the Jena CarboScope inversion system developed at the MPI for Biogeochemistry Jena (update of Rödenbeck, 2005; Rödenbeck et al., 2003). Atmospheric inversions estimate land- and ocean-atmosphere net carbon fluxes by minimizing a Bayesian cost function, which accounts for the

mismatch between observed and simulated atmospheric CO_2 mixing ratios. To do this, they use atmospheric CO_2 concentration at observation sites, combined with an atmospheric transport model as well as prior information on carbon emissions from fossil fuel burning and on carbon exchange between the atmosphere and land (and ocean). Detailed information inversions could be found in respective sources as mentioned above.

The CAMS inversion data (version r15v3) were provided for 1979-2015 with a weekly time-step and a spatial resolution of 1.875° latitude and 3.75° longitude. The Jena CarboScope inversion provides daily fluxes at a spatial resolution of 3.75° latitude and 5° longitude. It offers a series of runs that use differently large station sets with complete data coverage over time, in order to avoid spurious flux variations from a changing station network. From these runs, we used s04_v3.8 (shortened as Jena04 in the main text and supplementary material) using the largest number of measurement sites and therefore the most detailed constraint on carbon exchanges in 2015 (see http://www.bgc-jena.mpg.de/CarboScope/ for more details on other configurations). The s04_v3.8 run has a validity period as 2004–2015, although it does provide the data for the whole time span of 1981–2015. Site observations used over the validity period are coherent over time and it is optimal to examine the temporal trend within such a period. But results outside the validity period are still technically feasible and the temporal trend could thus be examined over the whole entire time span. We compared the linear trends over the larger latitudinal regions examined in this study between the s04_v3.8 and the long s81_v3.8 runs, and confirmed that the derived trends are similar. Therefore, in the calculation of the long-term linear trend used as a reference of interannual anomalies (see Sect. 2.2.2 below), we exceptionally use the s04_v3.8 run outside its period of validity. The CAMS inversion uses sites with at least 5-year worth of data. It therefore has a denser (during the recent decade) but temporally evolving data coverage than Carboscope. The evolving network in CAMS causes changes in inverted CO_2 fluxes that are superimposed on changes from biogeochemical drivers during the whole period.

In order to compare with the inversion data, land and ocean net carbon uptakes for 1981–2015 from the Global Carbon Project (Le Quéré et al., 2016) were used. For this purpose, an annual global carbon flux of 0.45 Pg C yr^{-1} is subtracted from the inversion-derived land carbon uptakes and is added to ocean carbon uptakes to account for the pre-industrial land-to-ocean carbon

fluxes induced by river transport (Jacobson et al., 2007), following Le Quéré et al. (2016). Estimates of ocean carbon uptake in GCP are based on observation-based mean CO_2 sink estimate for the 1990s and variability in the ocean CO_2 sink for 1959–2015 from global ocean biogeochemistry models. Estimates of land carbon uptake in GCP are calculated as the difference between anthropogenic emissions, atmospheric CO_2 growth and ocean sink. The estimates of land and ocean carbon uptake in GCP are largely independent from the two inversions used here, except that the CO_2 records from atmospheric stations which are used in inversions are also used in GCP to derive global AGR.

2.1.2 Atmospheric CO_2 growth rates, NDVI and climate data

Atmospheric CO_2 growth rates were retrieved from the Global Monitoring Division, Earth System Research Laboratory (ESRL), NOAA (http://www.esrl.noaa.gov/gmd/ccgg/trends/global.html). We used NDVI data between 2000 and 2015 from MODIS Terra Collection 6 (Didan, 2015), on a resolution of 0.05° and 16-day time step. NDVI data is processed from MODIS land surface reflectance data and thoroughly corrected for atmospheric effects. We strictly applied quality assurance (QA) controls to maintain distinct seasonal trajectory of vegetative radiometric observations and minimize spurious signals (e.g., snow or cloud). Detected unexpected non-vegetative observations were first excluded and then filled by the adaptive Savitzky–Golay filter (Chen et al., 2004; Jönsson and Eklundh, 2004). The Savitzky–Golay filter is a simplified convolution over a set of consecutive values with weighting coefficients given by a polynomial least-square-fit within the filter window (Savitzky and Golay, 1964). After this procedure, the linearly interpolated daily NDVI data was used to calculate mean seasonal NDVI and re-gridded at 0.5° resolution, with pixels of seasonal NDVI lower than 0.1 being further masked to ensure robustness. We examined four seasons: Q1 (January–March), Q2 (April–June), Q3 (July–September) and Q4 (October–December). Climate fields are from the ERA interim reanalysis (Dee et al., 2011) at 0.5° resolution and monthly time-step. We used air temperature, precipitation and volumetric soil water content (%) integrated over the soil column to a depth of 2.89 m.

2.1.3 Indices for El Niño–Southern Oscillation (ENSO) states and fire emission data

We examined the seasonal variations of the carbon cycle in 2015 in relation to ENSO events and

compared the 2015 El Niño event with that of 1997–1998. The Multivariate ENSO Index (MEI, http://www.esrl.noaa.gov/psd/enso/mei/, Wolter and Timlin, 2011) was used to indicate the ENSO state. MEI is a composite index calculated as the first un-rotated principal component of six ENSO-relevant variables (including sea level pressure and sea surface temperature) over the tropical Pacific for each of the twelve sliding bi-monthly seasons. MEI was widely used in previous studies as an indicator for ENSO states to examine land carbon dynamics (Nemani et al., 2003; van der Werf et al., 2008). The 12 bi-monthly MEI values of each year are summed to obtain the annual MEI. The interannual variations in climate and land carbon uptake are linked with MEI to infer general relationship between land carbon dynamics and ENSO climate oscillations. To examine the potential role of fire emissions in the land carbon balance in 2015, we used the GFED4s carbon emission data at daily time-step and 0.25° spatial resolution (http://www.globalfiredata.org/data.html). Monthly fire-carbon emissions were calculated for the regions and were examined for 1997–2015.

2.2 Data analysis

2.2.1 NDVI rank analysis and greening trend

Given a season and a pixel, the annual time series of seasonal NDVI for 2000-2015 were ranked in ascending order so that each year could be labelled by a rank, with 1 being the lowest and 16 being the highest. A spatial map of NDVI rank was then obtained for each year for the given season (Fig. S1). A composite map was made for year 2015, by merging pixels with the highest rank of all four seasons in 2015 (Fig. 1a). Vegetated area fraction with the highest rank for different years was obtained, with the sum of these fractions yielding unity. This procedure was repeated for all four seasons to generate four seasonal time series, with each containing the vegetation land fractions with highest NDVI for different years (Fig. 1b). It is noted that NDVI values for the northern hemisphere for Q1 and Q4 mostly fall outside the growing season (although October is frequently considered within the growing season and some evergreen coniferous forests show significant photosynthetic activities in March in regions of mild winter, e.g., Tanja et al., 2003), so that a valid NDVI might not necessarily be associated with significant seasonal vegetation activity. But as we applied a minimum value of 0.1 on seasonal NDVI, we expect that this issue is partly alleviated. Such seasonal segregation is adopted mainly because of its general applicability across the globe, especially for tropical ecosystems where seasonality in

vegetation activities is minimal.

2.2.2 Analysis of land carbon uptake dynamics associated with climate variations

Annual land and ocean carbon uptakes and carbon emissions from the two inversions were calculated for the globe over their period of overlap, 1981–2015. AGRs from NOAA/ESRL over 1981–2015 were converted into Pg C using a conversion factor of 2.12 Pg C ppm^{-1} (Ballantyne et al., 2012; Prather et al., 2012; Quéré et al., 2016) to examine the closure of the global carbon balance. The conversion factor used here assumes that the entire atmosphere is well mixed within one year. Because the record high AGR in 2015 was a composite effect collectively determined by carbon emissions from fossil fuel burning and industry, and land and ocean carbon uptakes, all being impacted by a historical trend (Fig. 2), it thus must be put into an historical perspective to reconcile evidence for extreme greening and the highest atmospheric CO_2 growth rate. For example, if 2015 comes up with a large increase in carbon emissions accompanied by droughts (browning) in the northern hemisphere and the tropics, then the highest AGR might not be regarded as a big surprise. Therefore, to understand the contributing factors for the highest AGR in 2015, we separated it into a long-term trend and interannual anomalies. For this reason, annual time series of carbon emissions, land and ocean carbon uptakes, and AGRs from NOAA/ESRL over 1981-2015 were linearly de-trended. The percentages of anomalies in carbon emissions, land and ocean sink in 2015 to the 2015 AGR anomaly were then calculated as relative contributions by each factor to the 2015 AGR anomaly.

Seasonal land carbon uptake anomaly time series were also calculated (the 0.45 Pg C yr^{-1} annual correction was not applied) by subtracting the same linear trend for 1981–2015. The globe was divided into three latitude bands: boreal Northern Hemisphere (BoNH, latitude > 45°N), temperate Northern Hemisphere (TeNH, 23.5° < latitude < 45°N), and tropics and extratropical Southern Hemisphere (TroSH, latitude < 23.5°N). The BoNH and TeNH are grouped as Boreal and temperate Northern Hemisphere (BoTeNH, latitude > 23.5°N) when examining seasonal carbon transitions. Seasonal land carbon uptake anomalies are then calculated for each region and the whole globe, with positive anomalies indicating enhanced sink (or reduced source) against the linear trend (i.e., the normal state), and negative ones indicating the opposite. The same seasonal linear de-trending was also performed for climate fields of air temperature,

precipitation and soil water content. The relationship between anomalies in land carbon uptake, temperature and precipitation are then examined using partial correlation coefficients in a multivariate linear regression framework with an ordinary least squares method. The relationship between seasonal land uptake anomalies and NDVI anomalies are also examined using simple linear regression.

We then examined especially the seasonal anomalies of land carbon uptake in 2015 and the carbon uptake transitions between two consecutive seasons, trying to reconcile extreme greening and a moderate land sink for this year. Seasonal land carbon uptake transitions are calculated as the land sink anomaly in a given season minus that of the previous one. When examining transitions of land carbon uptake anomalies by the CAMS inversion, we found the year 1993 has an extreme negative Q3→Q4 global transition (-2.85 Pg C within 6 months, $< -4\sigma$, the second lowest being the year 2015 with -1.0 Pg C) albeit with a reasonable annual land carbon uptake (3.75 Pg C yr^{-1}). This is linked with an extreme high Q3 and low Q4 uptake in this year, which could not be explained by any known carbon cycle mechanisms. This is thus identified as a result of numerical instability of the inversion system for that release and consequently the year 1993 has been removed from all the aforementioned seasonal analyses.

3 Results

3.1 Vegetation greening in 2015

Figure 1a illustrates where and when higher-than-normal greening conditions were observed in different seasons of the year 2015, compared to other years of 2000–2015 (see Supplementary Fig. S1 for greenness distribution for each season). On average over the four seasons of 2015, 16% of vegetated land shows record seasonal NDVI. The year with the second highest NDVI is 2014 with 9% vegetated area having record NDVI. An increase of the record-breaking NDVI occurrence over time is clearly seen in Fig. 1b. In short, 2015 clearly stands out as a greening outlier, having the highest proportion of vegetated land being the greenest for all four seasons except for the first season (despite the fact that for Q1, 2015 is still the third highest, Q1 = January to March).

For boreal and temperate regions of the Northern hemisphere, the seasons with highest NDVI in

2015 are dominated by Q2 and Q3 (Q2 = April to June; Q3 = July to September), corresponding to the growing season from spring to early autumn (Supplementary Fig. S2). A pronounced greening anomaly in Q2 occurred in western to central Siberia, western Canada and Alaska, and eastern and southern Asia (Supplementary Fig. S1). Central and eastern Siberia and eastern North America showed marked greening in Q3. Strong and widespread greening also occurred in the tropics during Q3 over Amazonia and the savanna (or cerrado) of eastern South America and tropical Africa, but this strong positive greening signal greatly diminished in Q4 (Q4 = October to December) especially over central to eastern Amazonia with the development of El Niño (Supplementary Fig. S1). The strongest greening in 2015 across the globe is overall dominated by the northern land (latitude > 23.5°N), while for the northern tropics (0–23.5°N) only moderately strong greening is found, and for the southern hemisphere the greening of 2015 is close to the average state of the period of 2000–2015 (Supplementary Fig. S3). The extreme growing-season greening in the northern land is confirmed by Bastos et al. (2017) as robust by using Terra MODIS NDVI data with different quality control procedures, and consistent between Terra and Aqua sensors (Fig. S1 in Bastos et al., 2017).

3.2 Global carbon balance for 1981-2015

Figure 2 shows the time series of fossil and industry carbon emissions, NOAA/ESRL AGR rates linked with ENSO climate oscillations as indicated by the Multivariate ENSO Index (MEI), and land and ocean carbon sinks for the common period of the two inversions (1981–2015) and the estimates by the Global Carbon Project (GCP). Emissions show a clear increase with time, however AGRs are more varying. The record high AGR of 2.96 ppm in 2015 exceeds those in all other previous years including the extreme El Niño event in 1997–98 despite much higher annual emissions in 2015. Interannual variability in AGR is mainly caused by fluctuations in land carbon sink, with Pearson's correlation coefficients between de-trended AGR and land sink < -0.8 ($p<0.01$) for both inversions (Pearson's correlation coefficient between de-trended AGR and MEI being 0.27, $p<0.1$). The root mean square differences between inversion and GCP carbon sinks are 0.70 and 0.65 Pg C yr^{-1} for CAMS and Jena04 respectively for the land, and ~0.5 PgC yr^{-1} for the ocean for both inversions, within the uncertainties of 0.8 and 0.5 Pg C yr^{-1} over 1981–2015, respectively for land and ocean as reported by GCP. The interannual variability of de-trended sink anomalies for the land agrees well between inversions and GCP (with Pearson's

correlation coefficient being 0.9 for both inversions, $p < 0.01$).

For 2015, the prescribed anthropogenic carbon emissions in the CAMS inversion are 9.9 Pg C yr^{-1}, of which 2.0 Pg C are absorbed by ocean, 1.7 Pg C by land ecosystems, with 6.2 Pg C remaining in the atmosphere, which matches the AGR from background stations of 6.3 Pg C assuming a conversion factor of 2.12 Pg C ppm^{-1} (Ballantyne et al., 2012; Le Quéré et al., 2016) and considering a measurement uncertainty of AGR as 0.09 ppm (0.2 Pg C) for 2015. When land carbon fluxes from the inversion are linearly de-trended over 1981-2015, the terrestrial sink in 2015 is by 1.2 Pg C lower than normal (i.e., the trend value), but this is not an extreme value — it is only the seventh weakest sink since 1981. This weaker land uptake accounts for 82% of the positive AGR anomaly, which is 1.45 Pg C in 2015 by subtracting a linear temporal trend. Jena04 yields an AGR in 2015 that is 0.13 ppm lower than the AGR based on background stations only, a difference close to the observation uncertainty. After removing the linear trends over time similarly as for the CAMS inversion, the land carbon uptake anomaly for Jena04 is -0.3 Pg C yr^{-1} in 2015, or 20% of the observed AGR anomaly, the remaining being explained by a positive anomaly in fossil fuel emissions (34%), a negative anomaly in the ocean sink (20%), and the difference between modelled AGR and NOAA/ESRL reported AGR. Note that the land sink by GCP for 2015 is much lower than in the two inversions, with de-trended anomaly lower than that of CAMS, indicating even larger contribution from land to the high anomaly of AGR.

In general, the warm phases of ENSO events are associated with positive anomalies in land air temperature, negative precipitation anomalies, and lower land carbon uptake anomalies (Fig. 3), consistent with previous studies (Cox et al., 2013; Wang et al., 2014). The lower precipitation during El Niño is due to a shift of precipitation from tropical land to the ocean (Adler et al., 2003), and higher land temperature might be due to reduction in evaporative cooling. The two extreme El Niño years of 1997 and 2015 have rather close MEI values. Compared with the 'standard' El Niño state of temperature and precipitation represented by the regression line, the year 1997 was relatively 'cool' and 'wet', while 2015 was rather 'warm' and 'dry' (with an extremely negative precipitation anomaly). Year 1998 has a smaller value of MEI than 1997/2015, but has a higher temperature anomaly than 2015, and a much lower land carbon uptake anomaly than 1997 and 2015 in both inversions, while the land carbon uptake anomalies

311 in 1997 and 2015 are similar. More detailed comparison of these three years and their carbon
312 cycle dynamics will be presented in the discussion section.
313
314 **3.3 Seasonal land carbon uptake dynamics associated with climate variations with a focus**
315 **on 2015**
316
317 The partial correlation coefficients between anomalies in seasonal land carbon uptake and those
318 in seasonal temperature and precipitation for different regions are shown in Fig. 4. The simple,
319 individual (univariate) linear relationships between de-trended anomalies in land carbon fluxes
320 and those in temperature and precipitation, are presented in Supplementary Fig. S4 and S5. Land
321 carbon fluxes show consistent relationships with temperature between the two inversions for
322 BoNH: positive relationship for Q2 and a negative one for the other three seasons (with Q1 by
323 Jena04 being the only insignificant one). Partial correlations between land fluxes and
324 precipitation are absent or non-significant for BoNH. This points to the fact that vegetation
325 productivity in BoNH is in principle dominated by temperature, with warmer spring and early
326 summer (Q2, April–June) enhancing vegetation net carbon uptake, but a higher temperature in
327 later summer, autumn and early winter mainly reduces the land capacity to sequester carbon,
328 consistent with previous studies (Piao et al., 2008). For TeNH, a significant negative relationship
329 is found between land fluxes by the CAMS inversion and temperature for Q3, and both
330 inversions show negative relationship between land fluxes and precipitation for Q4, probably due
331 to enhanced early autumn respiration under wetter conditions. For TroSH, land carbon uptakes in
332 Q1, Q2 and Q4 are all negatively related with temperature ($p<0.05$ for both inversions), while
333 increase in precipitation in Q1 is found to be associated with enhanced land uptake.
334
335 To explain the seeming paradox in 2015 between the strong greening and an only moderate
336 terrestrial uptake, we examined in detail the seasonal land carbon flux anomalies in 2015 (Fig. 5,
337 refer to Supplementary Fig. S6 for the spatial distribution of flux anomalies). At seasonal scale,
338 both inversions indicate positive carbon uptake anomalies during Q2 and Q3 for boreal and
339 temperate Northern Hemisphere (BoTeNH, latitude > 23.5°N), consistent with marked greening
340 in central to eastern Siberia, eastern Europe and Canada (Fig. 1) as outlined above. Indeed, both
341 BoNH and TeNH show positive relationships between seasonal land carbon flux anomalies and

342 NDVI anomalies for Q2 and Q3, with BoNH showing moderate greenness (after a linear trend
343 being removed) for Q3 and TeNH showing extreme greenness for Q2 in 2015 (Supplementary
344 Fig. S7). However, an extreme follow-up negative (source) anomaly occurred in Q4 (Fig. 5a).
345 These negative anomalies were lower than the 10th percentile of all anomalies in Q4 over time
346 for both inversions and they partly cancelled the extra uptake in Q2 and Q3. As a result, on the
347 annual time scale, the CAMS inversion shows an almost neutral land flux anomaly in BoTeNH,
348 while the Jena04 inversion still indicates a significant positive annual anomaly.
349
350 For the tropics and extratropical Southern Hemisphere (TroSH, latitude < 23.5°N), both
351 inversions show a weak negative land carbon anomaly for Q1 (mean value of -0.10 Pg C) in
352 2015, moderate anomalies in Q2 (of differing signs, with a negative one of -0.3 Pg C in CAMS
353 and a positive one of 0.2 Pg C in Jena04). Q3 anomalies are almost carbon neutral for both
354 inversions. In stark contrast, between Q3 and Q4, both inversions show a strong shift toward an
355 abnormally big land carbon source (i.e., negative anomalies of ~ -0.7 Pg C against a carbon
356 source expected from the linear trend, lower than 10th percentile over time in both inversions).
357 On the annual time scale, CAMS shows a large negative anomaly of -1.2 Pg C. For Jena04, sink
358 and source effects in Q1–Q3 cancelled each other, leaving the annual anomaly the same as in Q4.
359
360 Over the globe, the Jena04 inversion shows an abnormally strong sink during Q2 (normal state
361 being a net carbon sink), owing to synergy of enhanced Q2 uptakes in both BoTeNH and TroSH.
362 This abnormally enhanced uptake partly counteracted the strong shift toward source in Q4
363 (normal state being a net carbon source), leaving a small negative annual land carbon balance of
364 -0.3 Pg C. For the CAMS inversion, because of the co-occurrence of enhanced carbon release in
365 BoTeNH and the sudden shift toward a large carbon source in TroSH both in Q4 (normal states
366 being both net carbon sources), the land shows a strong global shift toward being a source in Q4,
367 leaving a negative annual carbon anomaly of -1.2 Pg C (i.e., carbon sink being reduced
368 compared with the normal state).
369
370 These consistent results from both inversions point to very strong seasonal shifts in the land
371 carbon balance as an emerging feature of 2015. We thus calculated ***transitions*** in land carbon
372 uptake anomaly as the first-order difference in flux anomalies between two consecutive seasons

(defined as the anomaly in a given season minus that in the previous one) for all years of the period 1982-2015 (Fig. 6). The ranks of transitions for different seasons relative to other years between the two inversions are broadly similar, except for Q1→Q2 and Q2→Q3 in TroSH, mainly due to the differences between the two inversions in seasonal land-carbon uptake anomaly in Q2 (Fig. 5b). On the global scale, both inversions show an extreme transition to a negative uptake anomaly for Q3→Q4, with 2015 being the largest transition of the period 1982-2015 (a transition towards an enhanced carbon source of -1.0 Pg C in 6 months). The abnormal transitions for Q3→Q4 on the global scale are located in the TroSH region, where both inversions show that during 1982-2015 the largest transition occurred in 2015. For BoTeNH, both inversions showed strong transitions toward positive anomaly for Q1→Q2; however, the same strong transition toward source anomaly occurred in Q3→Q4, partly cancelling the sink effects during growing seasons.

4 Discussion

4.1 Land carbon uptake dynamics with climate variations in northern latitudes and seasonal transitions of land carbon uptakes in 2015

The two inversions consistently allocate a strong positive carbon uptake anomaly in the region of BoTeNH during spring, which persists through the summer (Q2–Q3): an extreme sink anomaly is estimated in Q2 by Jena04, but a more moderate one by CAMS (still above the 75th percentile). The strong sinks in Q2 in both inversions are dominated by temperate Northern Hemisphere regions (TeNH, 23.5° < latitude < 45°N, Supplementary Fig. S8). For this region, both inversions show strong positive correlation between carbon uptake anomalies and NDVI in Q2, with an extremely high NDVI anomaly in 2015 (Supplementary Fig. S7f). Therefore, the strong sinks in Q2 are evidently linked with the extreme greening, although temperature and precipitation are only moderate (Fig. S4f, Fig. S5f).

For Q3, an extreme carbon sink anomaly occurs in boreal Northern Hemisphere (BoNH, latitude > 45°N) in CAMS; however, an equally strong negative anomaly (i.e., reduced sink) was found in TeNH in the same season, leaving the whole boreal and temperate Northern Hemisphere (BoTeNH) only a moderately enhanced sink anomaly (Fig. S8). Thus for TeNH alone, CAMS indicates extreme seasonal shift from a positive anomaly in Q2 to a negative one in Q3, implying

abrupt seasonal transitions probably resulting from enhanced ecosystem CO_2 release after growing-season uptake. For TeNH in 2015, NDVI persisted from a high extreme in Q2 to high values in Q3 (Fig. S7), and temperature remained moderate for both Q2 and Q3 (Fig. S4f, S4g), but precipitation shifted from a moderate anomaly in Q2 to an extremely low one (Fig. S5f, S5g). Therefore, the shift from a high Q2 sink anomaly to a big Q3 source anomaly by CAMS might be partly linked with the shift in precipitation and drought in Q3, such as the prevailing drought in Europe as shown in Fig. S9 (see also a detailed discussion of the European drought in Orth et al., 2016).

Inversion Jena04 agrees with a higher-than-normal sink in TeNH (23.5° < latitude < 45°N) during spring (Q2). It also reports a moderate positive anomaly for Q3 in BoNH, but does not show a strong negative anomaly (i.e., reduced sink) in TeNH in Q3 as CAMS does (Fig. S8). This is possibly related to differences in the measurement station data used, to different land prior fluxes (from the ORCHIDEE model in CAMS, and the LPJ model in Jena CarboScope), or to the fact that Jena inversion has a larger a-priori spatial error correlation length scale for its land fluxes (1275 km) than CAMS (500 km) (Chevallier et al., 2010; Rödenbeck et al., 2003). Nonetheless, both inversions consistently indicate that the enhancement of CO_2 uptake during spring and summer at the northern hemispheric scale was subsequently offset by an extreme source anomaly in autumn (Q4).

The large carbon source anomalies in Q4 shown by the two inversions in BoTeNH seem to be dominated by different factors in BoNH versus TeNH. In BoNH the source anomaly in 2015 is more linked with elevated temperature in Q4, which shows significant negative correlations with carbon uptake anomalies by both inversions (Fig. S4d). In contrast, precipitation in Q4 has no correlation with carbon uptake anomalies, and precipitation in 2015 was close to the normal state (Fig. S5d). The prevailing high temperature in Q4 of 2015 is especially evident over most of northern America, and central to eastern Siberia and Europe (Supplementary Fig. S9a).

In TeNH, the roles of temperate and precipitation are reversed compared to BoNH. Q4 precipitation is found to have significant negative correlation with land carbon uptake anomalies for both inversions, and Q4 in 2015 was characterized by a very high precipitation anomaly,

435 leading to reduced land carbon uptake (Fig. S5h). While temperature in Q4 of 2015 was
436 moderately high, no significant correlation is found between carbon uptake anomalies and
437 temperature (Fig. S4h). However, for both BoNH and TeNH, NDVI remained moderately high
438 in Q4 of 2015 (Fig. 7d, 7h).
439
440 The positive relationship between land carbon uptake and temperature in Q2 (spring and early
441 summer), and a negative one for Q3 and Q4 (autumn) for BoNH, are in line with previous
442 studies. Several studies reported an enhanced greening during spring and summer in the northern
443 hemisphere (Myneni et al., 1997; Zhou et al., 2001), as driven by increasing spring and summer
444 temperature (Barichivich et al., 2013; Nemani et al., 2003), leading to enhanced land carbon
445 uptake and a long-term increase in the seasonal amplitudes of atmospheric CO_2 in northern
446 latitudes (Forkel et al., 2016; Graven et al., 2013). However, for autumn, even though growing
447 season in autumn has been delayed because of autumn warming (Barichivich et al., 2013), land
448 carbon uptake termination time is found to have advanced as well, mainly due to enhanced
449 autumn respiration (Piao et al., 2008), which ultimately reduced net ecosystem carbon uptake
450 (Hadden and Grelle, 2016; Ueyama et al., 2014). For TeNH, we also found significant negative
451 relationship between land carbon uptake anomalies and temperature for Q3 using the CAMS
452 inversion data, consistent with the enhanced respiration by autumn warming found in
453 aforementioned studies. For Q4, however, both inversions point to decreasing land carbon
454 uptakes with increasing precipitation. This might be due to enhanced respiration by ameliorated
455 soil moisture condition, but this finding needs further examination on site scale in future studies.
456
457 For BoNH and TeNH, land carbon uptake anomalies are closely coupled with NDVI anomalies
458 for Q2 (positive correlation, albeit an insignificant one for TeNH Q2 using Jena04 data), but they
459 are generally de-coupled for Q3 and Q4, except that for Q3 of BoNH the CAMS-based land
460 carbon uptake show positive correlation with NDVI. This suggests high NDVI in autumn might
461 not necessarily relate to a high land carbon uptake. This is mainly because of two reasons. First,
462 NDVI is found to correlate well with leaf-level CO_2 uptake for deciduous forest for different
463 seasons, but is largely independent of leaf photosynthesis for evergreen forests (Gamon et al.,
464 1995). Second, even though a higher NDVI is associated with larger photosynthetic capacity and
465 a higher gross photosynthesis, autumn warming might increase ecosystem respiration more than

photosynthesis, leaving still a net carbon source effect. Furthermore, other studies also pointed out that severe summer drought can negate the enhanced carbon uptake during warm springs (Angert et al., 2005; Wolf et al., 2016).

4.2 Seasonal land carbon uptake transitions in the tropics and influences of El Niño and vegetation fire

The strong transition to abnormal source in the tropics and extratropical Southern Hemisphere was paralleled by a marked decrease in precipitation and an increase in temperature in Q4, with the development of El Niño in Q2–Q3 (Supplementary Fig. S4l, S5l, S10). Here El Niño development is indicated by the rise of the MEI and Oceanic Niño Index (ONI, http://www.cpc.ncep.noaa.gov/products/analysis_monitoring/ensostuff/ONI_change.shtml). This strong transition is consistent with the expected response of tropical and sub-tropical southern ecosystems during previous El Niño events (Ahlström et al., 2015; Cox et al., 2013; Poulter et al., 2014; Wang et al., 2013, 2014). The small abnormal source in Q1 in TroSH is consistent with a low precipitation anomaly. While temperature anomalies are abnormally high in Q2 and Q3, accompanied by extremely negative precipitation anomalies, the extremely low carbon flux in Q4 is largely explained by temperature, because correlations between land carbon uptake and precipitation in Q4 are very weak (Fig. S4i–l, Fig. S5i–l). Vegetation greenness has significant positive correlation with land carbon uptake anomalies for only Q1 in the tropics, and for the rest three seasons the correlation is very weak (Fig. S7i–l).

Compared with the 1997–98 El Niño, which was of similarly extreme magnitude, the 2015 El Niño started much earlier with positive MEI and ONI appearing during the first half of 2014. Since then until Q3 and Q4 in 2015 when El Niño began to reach its peak, the tropics and Southern Hemisphere saw continuous higher-than-normal temperatures, with continually decreasing precipitation and accumulating deficit in soil water content (Supplementary Fig. S10). From Q3 to Q4, a steep decline is further observed in both precipitation and soil moisture with stagnating high temperature anomaly, which is probably a major cause of the strong shift toward a carbon source anomaly. The CAMS inversion shows a carbon source anomaly in Q4 of 2015 slightly smaller than that in Q3 of 1997, while the Jena04 inversion shows almost equal

497 magnitudes of loss in land sink strength between these two extreme El Niño events. On the one
498 hand, El Niño in late 2015 started with an early onset and built upon the cumulative effects of the
499 drought since the beginning of the year; it thus came with larger negative anomaly in
500 precipitation and soil water content than the 1997–98 El Niño. This sequence of events might
501 favour a stronger land carbon source. On the other hand, the fire emission anomaly in the tropics
502 in 2015 was less than half of that in 1997 at the peak of El Niño (Fig. S10), which might
503 contribute to a smaller land source anomaly in 2015 than in 1997–98.
504
505 El Niño events are usually associated with increased vegetation fires, and these have a large
506 impact on the global carbon cycle (van der Werf et al., 2004). Global fire emissions of carbon
507 reached 3.0 and 2.9 Pg C in 1997 and 1998 according to the GFED4s data. These two years
508 produced the largest source of fire-emitted carbon for the entire period 1997–2015. Global fire
509 emissions in 2015 reached 2.3 Pg C, close to the 1997-2015 average (2.2 Pg C yr^{-1}) but 23–24%
510 lower than 1997–98 — the difference mainly occurring in the southern tropics (0–23.5°S, Fig.
511 S10). In particular, carbon emissions from deforestation and peat fires were two times lower in
512 2015 (0.6 Pg C) compared with 1997 (1.2 Pg C) (GFED4s data), and emissions for these types of
513 fires are more likely to be a net source contribution, because they cannot be compensated by
514 vegetation regrowth within a short time. Fire emission data thus suggests a smaller contribution
515 from fires to AGR in 2015 than 1997–98. If both annual time series of AGR and global fire-
516 carbon emissions are de-trended within their overlapping period of 1997-2015, fire-carbon
517 emissions have an anomaly of 0.4 Pg C yr^{-1} in 2015, explaining only 29% of the AGR anomaly.
518
519 There has been a long debate on whether tropical vegetations show enhanced greenness as
520 indicated by vegetation indices (i.e., NDVI and enhanced vegetation index or EVI) during dry
521 seasons or drought periods in tropical forest (Huete et al., 2006; Morton et al., 2014; Saleska et
522 al., 2007; Samanta et al., 2010; Xu et al., 2011), and whether there is an accompanying decrease
523 in long-term vegetation productivity associated with droughts (Medlyn, 2011; Samanta et al.,
524 2011; Zhao and Running, 2010). Some studies show enhanced green-up in Amazonian forest
525 during dry seasons mainly due to the release of radiation control on vegetation activities (Huete
526 et al., 2006; Zhao and Running, 2010), while Samanta et al. (2010) argued such observed green-
527 up is an artefact of atmosphere-corrupted data. A recent study by Morton et al. (2014) rather

argued that if errors of satellite observation angle are corrected, no increase in EVI could be observed during dry seasons.

While forest plot level data demonstrated consistent negative effect of droughts on tropical carbon uptake mainly through enhanced tree mortality (Lewis et al., 2011; Phillips et al., 2009), site level observations failed to see immediate reduction in forest net primary productivity (Doughty et al., 2015) or even saw increased gross photosynthesis or photosynthesis capacity when dry seasons initiate (Huete et al., 2006; Wu et al., 2016). Further, a large mortality event for trees will cause a legacy source over several years rather than a rapid release of CO_2 to the atmosphere during the year when trees died.

Both Wang et al. (2013) and Wang et al. (2014) found a higher correlation coefficient between interannual variability in tropical land carbon fluxes (as inferred from interannual variations in AGR) of temperature than precipitation, which is confirmed by our analysis of inversion-based tropical land flux anomalies with climate variations (Fig 4). However, forest plot level observations point to the prevailing drought as the dominant factor to reduce forest carbon storage (Phillips et al., 2009). It remains challenging to reconcile the findings of temperature dominance at large spatial scale and precipitation/moisture dominance at fine scale. Recently, Jung et al. (2017) suggested that the dominant role of soil moisture over land carbon flux anomalies has shifted to temperature when the scale of spatial aggregation increases, due to the compensatory water effects in spatial upscaling. We also find that for all seasons except Q3, inversion-based land carbon uptake anomalies in the tropics and southern extratropics are positively correlated with soil water content, with 2015 having an extreme low soil water content anomaly in Q4 (data not shown), echoing the extreme high temperature anomaly shown in Fig. S4l. This might indicate that temperature impacts the land carbon uptake mainly by increasing evaporative demand and decreasing soil water content. Besides, except Q1, we found no strong link between seasonal land carbon uptake anomalies and NDVI anomalies.

4.3 Data uncertainties and perspective

On the global and hemispheric scales, the inversion-derived land- and ocean-atmosphere fluxes are well constrained by the observed atmospheric CO_2 growth rates on measurement sites.

559 However, because the observational network is heterogeneous and sites are sparsely distributed
560 (Supplementary Fig. S11), land CO_2 fluxes cannot be resolved precisely over each grid cell
561 (Kaminski et al., 2001) and some regions are better constrained than others. This could hinder
562 the precise pixel-scale matching between gridded CO_2 flux maps and climate states or the
563 occurrence of climate extremes to investigate how climate extreme impact carbon fluxes.
564 Although we have identified carbon uptake transitions for some regions and seasons might be
565 related with certain climate extremes (e.g., the role of precipitation in TeNH of Q4 shown in Fig.
566 S5h), but in general exact attribution of carbon uptake transitions into different climate drivers
567 could be elusive. Further, a few other uncertainties matter for the specific objective of this study.
568 First, the atmospheric network increased over time, so that the inversions have a better ability to
569 detect and quantify a sharp transition in CO_2 fluxes occurring in the last than in the first decade
570 of the period analysed. This might hide the detection of other more extreme end-of-year carbon
571 transitions during early years of our target period (1981-2015). Second, because measurements
572 for the early 2016 are not used in the CAMS inversion and not completely available in the Jena
573 inversion, the constraining of last season in 2015 is weaker than for the other three seasons. This
574 could partly influence the exact magnitude of the extreme Q4 negative anomaly in land carbon
575 uptake reported here. Third, the sparse sites located in the boreal Eurasia and tropical regions
576 might diminish the ability of inversion systems to robustly allocation carbon fluxes spatially,
577 which could yield high uncertainty in the carbon fluxes diagnosed for these regions (van der
578 Laan-Luijkx et al., 2015; Stephens et al., 2007).
579
580 Despite these uncertainties, the strong transition of CO_2 fluxes from Q3 to Q4 analysed here is
581 the largest ever found in the inversion records. Although 2015 shows extreme greening in the
582 northern hemisphere, this strong greenness has been only translated into a moderate annual
583 carbon sink anomaly in 2015, because vegetation greenness and land uptake anomalies are
584 largely decoupled outside growing season. The strong transition to carbon source in TeNH in Q4
585 is consistent with extreme precipitation that might have largely increased respiration loss. In the
586 tropics, the transition to a strong source in TroSH in Q4 is congruent with the expected response
587 of ecosystems to the peak of an El Niño event. However, given the ambiguous findings regarding
588 changes in vegetation greenness during dry seasons or drought periods by previous studies
589 (Saleska et al., 2007; Xu et al., 2011), and the uncertain roles of climate variations in driving the

590 regional land carbon balance, more work is needed to reveal how these processes have evolved
591 during opposing ENSO events. For the boreal and temperate Northern Hemisphere, further
592 investigation is still needed to verify whether a coupling between strong spring/summer uptake
593 and autumn release is something intrinsic to natural ecosystems, or if strong transitions to
594 autumn release are triggered more by abrupt climate shifts. This could be evaluated by process-
595 based and data-driven models to partition the overall sink anomaly into individual responses of
596 photosynthesis and respiration, but that is beyond the scope of this work. Our results point to the
597 need to better understand the drivers of carbon dynamics at seasonal, or even shorter time scales
598 at the regional to global level, especially the link between such dynamics and climate extremes.
599 Such understanding would help better predictions of the response of the carbon cycle to multiple
600 long-term drivers such as atmospheric CO_2 growth and climate change.
601
602 **5 Conclusions**
603 We investigated the links among vegetation greenness, interannual land carbon flux variations
604 and climate variations for 1981–2015 using inversion-based land carbon flux data sets.
605 Consistent positive correlations between satellite-derived vegetation greenness and land carbon
606 uptakes are found for the northern hemisphere during growing season, but outside the growing
607 season, vegetation greenness and land carbon uptake are largely decoupled. Carbon uptake in the
608 boreal northern hemisphere (>45°N) is more consistently associated with temperature than
609 precipitation, while such a pattern is less evident for the temperate northern hemisphere (23.5–
610 45°N). Consistent with previous studies, we found a strong negative impact by temperature in
611 the land carbon uptakes in tropics and southern hemisphere, probably driven by the role of
612 temperature in soil water content.
613
614 We made an emphasis on the seasonal dynamics of land carbon uptake in 2015 due to its
615 seeming paradox between the greatest vegetation greenness and the highest atmospheric CO_2
616 growth rate. We found that lands in Northern Hemisphere started with a higher-than-normal sink
617 for the northern growing seasons, consistent with enhanced vegetation greenness partly owing to
618 elevated warming, however this enhanced sink was partly balanced by enhanced carbon release
619 in autumn and winter, associated with extremely high precipitation in Q4 in temperate northern
620 hemisphere (23.5–45°N). For tropics and Southern Hemisphere, a strong and abrupt transition

toward a large carbon source for the last quarter of 2015 was found, concomitant with the peak of El Niño development. This strong transition of terrestrial CO2 fluxes in the last quarter is the largest in the inversion records since 1981. The transitions in CO_2 fluxes diagnosed in this study form an interesting test bed for evaluating ecosystem models and gaining understanding of their controlling processes.

References

Adler, R. F., Huffman, G. J., Chang, A., Ferraro, R., Xie, P.-P., Janowiak, J., Rudolf, B., Schneider, U., Curtis, S., Bolvin, D., Gruber, A., Susskind, J., Arkin, P. and Nelkin, E.: The Version-2 Global Precipitation Climatology Project (GPCP) Monthly Precipitation Analysis (1979–Present), J. Hydrometeorol., 4(6), 1147–1167, doi:10.1175/1525-7541(2003)004<1147:TVGPCP>2.0.CO;2, 2003.

Ahlström, A., Raupach, M. R., Schurgers, G., Smith, B., Arneth, A., Jung, M., Reichstein, M., Canadell, J. G., Friedlingstein, P., Jain, A. K., Kato, E., Poulter, B., Sitch, S., Stocker, B. D., Viovy, N., Wang, Y. P., Wiltshire, A., Zaehle, S. and Zeng, N.: The dominant role of semi-arid ecosystems in the trend and variability of the land CO2 sink, Science, 348(6237), 895–899, doi:10.1126/science.aaa1668, 2015.

Angert, A., Biraud, S., Bonfils, C., Henning, C. C., Buermann, W., Pinzon, J., Tucker, C. J. and Fung, I.: Drier summers cancel out the CO2 uptake enhancement induced by warmer springs, Proc. Natl. Acad. Sci. U. S. A., 102(31), 10823–10827, doi:10.1073/pnas.0501647102, 2005.

Ballantyne, A. P., Alden, C. B., Miller, J. B., Tans, P. P. and White, J. W. C.: Increase in observed net carbon dioxide uptake by land and oceans during the past 50 years, Nature, 488(7409), 70–72, doi:10.1038/nature11299, 2012.

Barichivich, J., Briffa, K. R., Myneni, R. B., Osborn, T. J., Melvin, T. M., Ciais, P., Piao, S. and Tucker, C.: Large-scale variations in the vegetation growing season and annual cycle of atmospheric CO2 at high northern latitudes from 1950 to 2011, Glob. Change Biol., 19(10), 3167–3183, doi:10.1111/gcb.12283, 2013.

Bastos, A., Ciais, P., Park, T., Zscheischler, J., Yue, C., Barichivich, J., Myneni, R. B., Peng, S., Piao, S. and Zhu, Z.: Was the extreme Northern Hemisphere greening in 2015 predictable?, Environ. Res. Lett., 12(4), 044016, doi:10.1088/1748-9326/aa67b5, 2017.

Canadell, J. G., Le Quéré, C., Raupach, M. R., Field, C. B., Buitenhuis, E. T., Ciais, P., Conway, T. J., Gillett, N. P., Houghton, R. A. and Marland, G.: Contributions to accelerating atmospheric CO2 growth from economic activity, carbon intensity, and efficiency of natural sinks, Proc. Natl. Acad. Sci., 104(47), 18866–18870, 2007.

Chen, J., Jönsson, P., Tamura, M., Gu, Z., Matsushita, B. and Eklundh, L.: A simple method for reconstructing a high-quality NDVI time-series data set based on the Savitzky–Golay filter, Remote Sens. Environ., 91(3), 332–344, doi:10.1016/j.rse.2004.03.014, 2004.

Chevallier, F., Fisher, M., Peylin, P., Serrar, S., Bousquet, P., Bréon, F.-M., Chédin, A. and Ciais, P.: Inferring CO2 sources and sinks from satellite observations: Method and application to TOVS data, J. Geophys. Res. Atmospheres, 110(D24), D24309, doi:10.1029/2005JD006390, 2005.

Chevallier, F., Ciais, P., Conway, T. J., Aalto, T., Anderson, B. E., Bousquet, P., Brunke, E. G., Ciattaglia, L., Esaki, Y., Fröhlich, M., Gomez, A., Gomez-Pelaez, A. J., Haszpra, L., Krummel, P. B., Langenfelds, R. L., Leuenberger, M., Machida, T., Maignan, F., Matsueda, H., Morguí, J. A., Mukai, H., Nakazawa, T., Peylin, P., Ramonet, M., Rivier, L., Sawa, Y., Schmidt, M., Steele, L. P., Vay, S. A., Vermeulen, A. T., Wofsy, S. and Worthy, D.: CO2 surface fluxes at grid point scale estimated from a global 21 year reanalysis of atmospheric measurements, J. Geophys. Res. Atmospheres, 115(D21), D21307, doi:10.1029/2010JD013887, 2010.

Cox, P. M., Pearson, D., Booth, B. B., Friedlingstein, P., Huntingford, C., Jones, C. D. and Luke, C. M.: Sensitivity of tropical carbon to climate change constrained by carbon dioxide variability, Nature, 494(7437), 341–344, doi:10.1038/nature11882, 2013.

Dee, D. P., Uppala, S. M., Simmons, A. J., Berrisford, P., Poli, P., Kobayashi, S., Andrae, U., Balmaseda, M. A., Balsamo, G., Bauer, P., Bechtold, P., Beljaars, A. C. M., van de Berg, L., Bidlot, J., Bormann, N., Delsol, C., Dragani, R., Fuentes, M., Geer, A. J., Haimberger, L., Healy, S. B., Hersbach, H., Hólm, E. V., Isaksen, L., Kållberg, P., Köhler, M., Matricardi, M., McNally, A. P., Monge-Sanz, B. M., Morcrette, J.-J., Park, B.-K., Peubey, C., de Rosnay, P., Tavolato, C., Thépaut, J.-N. and Vitart, F.: The ERA-Interim reanalysis: configuration and performance of the data assimilation system, Q. J. R. Meteorol. Soc., 137(656), 553–597, doi:10.1002/qj.828, 2011.

Didan K 2015 MOD13C1 MODIS/Terra Vegetation Indices 16-Day L3 Global 0.05Deg CMG V006 NASA EOSDIS Land Processes DAAC (https://doi.org/10.5067/MODIS/ MOD13C1.006)

Doughty, C. E., Metcalfe, D. B., Girardin, C. a. J., Amézquita, F. F., Cabrera, D. G., Huasco, W. H., Silva-Espejo, J. E., Araujo-Murakami, A., da Costa, M. C., Rocha, W., Feldpausch, T. R., Mendoza, A. L. M., da Costa, A. C. L., Meir, P., Phillips, O. L. and Malhi, Y.: Drought impact on forest carbon dynamics and fluxes in Amazonia, Nature, 519(7541), 78–82, doi:10.1038/nature14213, 2015.

Forkel, M., Carvalhais, N., Rödenbeck, C., Keeling, R., Heimann, M., Thonicke, K., Zaehle, S. and Reichstein, M.: Enhanced seasonal CO2 exchange caused by amplified plant productivity in northern ecosystems, Science, 351(6274), 696–699, doi:10.1126/science.aac4971, 2016.

Gamon, J. A., Field, C. B., Goulden, M. L., Griffin, K. L., Hartley, A. E., Joel, G., Peñuelas, J. and Valentini, R.: Relationships Between NDVI, Canopy Structure, and Photosynthesis in Three Californian Vegetation Types, Ecol. Appl., 5(1), 28–41, doi:10.2307/1942049, 1995.

Graven, H. D., Keeling, R. F., Piper, S. C., Patra, P. K., Stephens, B. B., Wofsy, S. C., Welp, L. R., Sweeney, C., Tans, P. P., Kelley, J. J., Daube, B. C., Kort, E. A., Santoni, G. W. and Bent, J. D.: Enhanced Seasonal Exchange of CO2 by Northern Ecosystems Since 1960, Science, 341(6150), 1085–1089, doi:10.1126/science.1239207, 2013.

Gu, L., Baldocchi, D. D., Wofsy, S. C., Munger, J. W., Michalsky, J. J., Urbanski, S. P. and Boden, T. A.: Response of a Deciduous Forest to the Mount Pinatubo Eruption: Enhanced Photosynthesis, Science, 299(5615), 2035–2038, doi:10.1126/science.1078366, 2003.

Hadden, D. and Grelle, A.: Changing temperature response of respiration turns boreal forest from carbon sink into carbon source, Agric. For. Meteorol., 223, 30–38, doi:10.1016/j.agrformet.2016.03.020, 2016.

Huete, A. R., Didan, K., Shimabukuro, Y. E., Ratana, P., Saleska, S. R., Hutyra, L. R., Yang, W., Nemani, R. R. and Myneni, R.: Amazon rainforests green-up with sunlight in dry season, Geophys. Res. Lett., 33(6), L06405, doi:10.1029/2005GL025583, 2006.

Huijnen, V., Wooster, M. J., Kaiser, J. W., Gaveau, D. L. A., Flemming, J., Parrington, M., Inness, A., Murdiyarso, D., Main, B. and Weele, M. van: Fire carbon emissions over maritime southeast Asia in 2015 largest since 1997, Sci. Rep., 6, 26886, doi:10.1038/srep26886, 2016.

Jacobson, A. R., Mikaloff Fletcher, S. E., Gruber, N., Sarmiento, J. L. and Gloor, M.: A joint atmosphere-ocean inversion for surface fluxes of carbon dioxide: 1. Methods and global-scale fluxes, Glob. Biogeochem. Cycles, 21(1), GB1019, doi:10.1029/2005GB002556, 2007.

Jiménez-Muñoz, J. C., Mattar, C., Barichivich, J., Santamaría-Artigas, A., Takahashi, K., Malhi, Y., Sobrino, J. A. and Schrier, G. van der: Record-breaking warming and extreme drought in the Amazon rainforest during the course of El Niño 2015–2016, Sci. Rep., 6, 33130, doi:10.1038/srep33130, 2016.

Jönsson, P. and Eklundh, L.: TIMESAT—a program for analyzing time-series of satellite sensor data, Comput. Geosci., 30(8), 833–845, doi:10.1016/j.cageo.2004.05.006, 2004.

Jung, M., Reichstein, M., Schwalm, C. R., Huntingford, C., Sitch, S., Ahlström, A., Arneth, A., Camps-

714 Valls, G., Ciais, P., Friedlingstein, P. and others: Compensatory water effects link yearly global land
715 CO2 sink changes to temperature, Nature [online] Available from:
716 https://www.nature.com/nature/journal/vaop/ncurrent/full/nature20780.html (Accessed 19 June 2017),
717 2017.
718 Kaminski, T., Rayner, P. J., Heimann, M. and Enting, I. G.: On aggregation errors in atmospheric
719 transport inversions, J. Geophys. Res. Atmospheres, 106(D5), 4703–4715,
720 doi:10.1029/2000JD900581, 2001.
721 van der Laan-Luijkx, I. T., van der Velde, I. R., Krol, M. C., Gatti, L. V., Domingues, L. G., Correia, C.
722 S. C., Miller, J. B., Gloor, M., van Leeuwen, T. T., Kaiser, J. W., Wiedinmyer, C., Basu, S., Clerbaux,
723 C. and Peters, W.: Response of the Amazon carbon balance to the 2010 drought derived with
724 CarbonTracker South America, Glob. Biogeochem. Cycles, 29(7), 2014GB005082,
725 doi:10.1002/2014GB005082, 2015.
726 Lewis, S. L., Brando, P. M., Phillips, O. L., van der Heijden, G. M. and Nepstad, D.: The 2010 amazon
727 drought, Science, 331(6017), 554–554, 2011.
728 Li, W., Ciais, P., Wang, Y., Peng, S., Broquet, G., Ballantyne, A. P., Canadell, J. G., Cooper, L.,
729 Friedlingstein, P., Quéré, C. L., Myneni, R. B., Peters, G. P., Piao, S. and Pongratz, J.: Reducing
730 uncertainties in decadal variability of the global carbon budget with multiple datasets, Proc. Natl.
731 Acad. Sci., 113(46), 13104–13108, doi:10.1073/pnas.1603956113, 2016.
732 Medlyn, B. E.: Comment on "Drought-Induced Reduction in Global Terrestrial Net Primary Production
733 from 2000 Through 2009," Science, 333(6046), 1093–1093, doi:10.1126/science.1199544, 2011.
734 Morton, D. C., Nagol, J., Carabajal, C. C., Rosette, J., Palace, M., Cook, B. D., Vermote, E. F., Harding,
735 D. J. and North, P. R. J.: Amazon forests maintain consistent canopy structure and greenness during
736 the dry season, Nature, 506(7487), 221–224, doi:10.1038/nature13006, 2014.
737 Myneni, R. B., Keeling, C. D., Tucker, C. J., Asrar, G. and Nemani, R. R.: Increased plant growth in the
738 northern high latitudes from 1981 to 1991, Nature, 386(6626), 698–702, doi:10.1038/386698a0, 1997.
739 Nemani, R. R., Keeling, C. D., Hashimoto, H., Jolly, W. M., Piper, S. C., Tucker, C. J., Myneni, R. B.
740 and Running, S. W.: Climate-Driven Increases in Global Terrestrial Net Primary Production from
741 1982 to 1999, Science, 300(5625), 1560–1563, doi:10.1126/science.1082750, 2003.
742 Orth, R., Zscheischler, J. and Seneviratne, S. I.: Record dry summer in 2015 challenges precipitation
743 projections in Central Europe, Sci. Rep., 6, 28334, doi:10.1038/srep28334, 2016.
744 Phillips, O. L., Aragão, L. E. O. C., Lewis, S. L., Fisher, J. B., Lloyd, J., López-González, G., Malhi, Y.,
745 Monteagudo, A., Peacock, J., Quesada, C. A., Heijden, G. van der, Almeida, S., Amaral, I., Arroyo,
746 L., Aymard, G., Baker, T. R., Bánki, O., Blanc, L., Bonal, D., Brando, P., Chave, J., Oliveira, Á. C. A.
747 de, Cardozo, N. D., Czimczik, C. I., Feldpausch, T. R., Freitas, M. A., Gloor, E., Higuchi, N., Jiménez,
748 E., Lloyd, G., Meir, P., Mendoza, C., Morel, A., Neill, D. A., Nepstad, D., Patiño, S., Peñuela, M. C.,
749 Prieto, A., Ramírez, F., Schwarz, M., Silva, J., Silveira, M., Thomas, A. S., Steege, H. ter, Stropp, J.,
750 Vásquez, R., Zelazowski, P., Dávila, E. A., Andelman, S., Andrade, A., Chao, K.-J., Erwin, T., Fiore,
751 A. D., C, E. H., Keeling, H., Killeen, T. J., Laurance, W. F., Cruz, A. P., Pitman, N. C. A., Vargas, P.
752 N., Ramírez-Angulo, H., Rudas, A., Salamão, R., Silva, N., Terborgh, J. and Torres-Lezama, A.:
753 Drought Sensitivity of the Amazon Rainforest, Science, 323(5919), 1344–1347,
754 doi:10.1126/science.1164033, 2009.
755 Piao, S., Ciais, P., Friedlingstein, P., Peylin, P., Reichstein, M., Luyssaert, S., Margolis, H., Fang, J., Barr,
756 A., Chen, A., Grelle, A., Hollinger, D. Y., Laurila, T., Lindroth, A., Richardson, A. D. and Vesala, T.:
757 Net carbon dioxide losses of northern ecosystems in response to autumn warming, Nature, 451(7174),

758 49–52, doi:10.1038/nature06444, 2008.
759 Piao, S., Nan, H., Huntingford, C., Ciais, P., Friedlingstein, P., Sitch, S., Peng, S., Ahlström, A., Canadell,
760 J. G., Cong, N., Levis, S., Levy, P. E., Liu, L., Lomas, M. R., Mao, J., Myneni, R. B., Peylin, P.,
761 Poulter, B., Shi, X., Yin, G., Viovy, N., Wang, T., Wang, X., Zaehle, S., Zeng, N., Zeng, Z. and Chen,
762 A.: Evidence for a weakening relationship between interannual temperature variability and northern
763 vegetation activity, Nat. Commun., 5, 5018, doi:10.1038/ncomms6018, 2014.
764 Poulter, B., Frank, D., Ciais, P., Myneni, R. B., Andela, N., Bi, J., Broquet, G., Canadell, J. G.,
765 Chevallier, F., Liu, Y. Y., Running, S. W., Sitch, S. and van der Werf, G. R.: Contribution of semi-arid
766 ecosystems to interannual variability of the global carbon cycle, Nature, 509(7502), 600–603,
767 doi:10.1038/nature13376, 2014.
768 Prather, M. J., Holmes, C. D. and Hsu, J.: Reactive greenhouse gas scenarios: Systematic exploration of
769 uncertainties and the role of atmospheric chemistry, Geophys. Res. Lett., 39(9), L09803,
770 doi:10.1029/2012GL051440, 2012.
771 Quéré, C. L., Andrew, R. M., Canadell, J. G., Sitch, S., Korsbakken, J. I., Peters, G. P., Manning, A. C.,
772 Boden, T. A., Tans, P. P., Houghton, R. A., Keeling, R. F., Alin, S., Andrews, O. D., Anthoni, P.,
773 Barbero, L., Bopp, L., Chevallier, F., Chini, L. P., Ciais, P., Currie, K., Delire, C., Doney, S. C.,
774 Friedlingstein, P., Gkritzalis, T., Harris, I., Hauck, J., Haverd, V., Hoppema, M., Klein Goldewijk, K.,
775 Jain, A. K., Kato, E., Körtzinger, A., Landschützer, P., Lefèvre, N., Lenton, A., Lienert, S.,
776 Lombardozzi, D., Melton, J. R., Metzl, N., Millero, F., Monteiro, P. M. S., Munro, D. R., Nabel, J. E.
777 M. S., Nakaoka, S., O'Brien, K., Olsen, A., Omar, A. M., Ono, T., Pierrot, D., Poulter, B., Rödenbeck,
778 C., Salisbury, J., Schuster, U., Schwinger, J., Séférian, R., Skjelvan, I., Stocker, B. D., Sutton, A. J.,
779 Takahashi, T., Tian, H., Tilbrook, B., Laan-Luijkx, I. T. van der, Werf, G. R. van der, Viovy, N.,
780 Walker, A. P., Wiltshire, A. J. and Zaehle, S.: Global Carbon Budget 2016, Earth Syst. Sci. Data, 8(2),
781 605–649, doi:10.5194/essd-8-605-2016, 2016.
782 Rödenbeck, C.: Estimating CO2 sources and sinks from atmospheric mixing ratio measurements using a
783 global inversion of atmospheric transport, Max Planck Institute for Biogeochemistry., 2005.
784 Rödenbeck, C., Houweling, S., Gloor, M. and Heimann, M.: CO2 flux history 1982–2001 inferred from
785 atmospheric data using a global inversion of atmospheric transport, Atmos Chem Phys, 3(6), 1919–
786 1964, doi:10.5194/acp-3-1919-2003, 2003.
787 Saleska, S. R., Didan, K., Huete, A. R. and Rocha, H. R. da: Amazon Forests Green-Up During 2005
788 Drought, Science, 318(5850), 612–612, doi:10.1126/science.1146663, 2007.
789 Samanta, A., Ganguly, S., Hashimoto, H., Devadiga, S., Vermote, E., Knyazikhin, Y., Nemani, R. R. and
790 Myneni, R. B.: Amazon forests did not green-up during the 2005 drought, Geophys. Res. Lett., 37(5),
791 L05401, doi:10.1029/2009GL042154, 2010.
792 Samanta, A., Costa, M. H., Nunes, E. L., Vieira, S. A., Xu, L. and Myneni, R. B.: Comment on "Drought-
793 Induced Reduction in Global Terrestrial Net Primary Production from 2000 Through 2009," Science,
794 333(6046), 1093–1093, doi:10.1126/science.1199048, 2011.
795 Stephens, B. B., Gurney, K. R., Tans, P. P., Sweeney, C., Peters, W., Bruhwiler, L., Ciais, P., Ramonet,
796 M., Bousquet, P., Nakazawa, T., Aoki, S., Machida, T., Inoue, G., Vinnichenko, N., Lloyd, J., Jordan,
797 A., Heimann, M., Shibistova, O., Langenfelds, R. L., Steele, L. P., Francey, R. J. and Denning, A. S.:
798 Weak Northern and Strong Tropical Land Carbon Uptake from Vertical Profiles of Atmospheric CO2,
799 Science, 316(5832), 1732–1735, doi:10.1126/science.1137004, 2007.
800 Tanja, S., Berninger, F., Vesala, T., Markkanen, T., Hari, P., Mäkelä, A., Ilvesniemi, H., Hänninen, H.,
801 Nikinmaa, E., Huttula, T., Laurila, T., Aurela, M., Grelle, A., Lindroth, A., Arneth, A., Shibistova, O.

and Lloyd, J.: Air temperature triggers the recovery of evergreen boreal forest photosynthesis in spring, Glob. Change Biol., 9(10), 1410–1426, doi:10.1046/j.1365-2486.2003.00597.x, 2003.
Ueyama, M., Iwata, H. and Harazono, Y.: Autumn warming reduces the CO2 sink of a black spruce forest in interior Alaska based on a nine-year eddy covariance measurement, Glob. Change Biol., 20(4), 1161–1173, doi:10.1111/gcb.12434, 2014.
Wang, W., Ciais, P., Nemani, R. R., Canadell, J. G., Piao, S., Sitch, S., White, M. A., Hashimoto, H., Milesi, C. and Myneni, R. B.: Variations in atmospheric CO2 growth rates coupled with tropical temperature, Proc. Natl. Acad. Sci., 110(32), 13061–13066, doi:10.1073/pnas.1219683110, 2013.
Wang, X., Piao, S., Ciais, P., Friedlingstein, P., Myneni, R. B., Cox, P., Heimann, M., Miller, J., Peng, S., Wang, T., Yang, H. and Chen, A.: A two-fold increase of carbon cycle sensitivity to tropical temperature variations, Nature, 506(7487), 212–215, doi:10.1038/nature12915, 2014.
van der Werf, G. R., Randerson, J. T., Collatz, G. J., Giglio, L., Kasibhatla, P. S., Arellano, A. F., Olsen, S. C. and Kasischke, E. S.: Continental-Scale Partitioning of Fire Emissions During the 1997 to 2001 El Niño/La Niña Period, Science, 303(5654), 73–76, doi:10.1126/science.1090753, 2004.
van der Werf, G. R., Dempewolf, J., Trigg, S. N., Randerson, J. T., Kasibhatla, P. S., Giglio, L., Murdiyarso, D., Peters, W., Morton, D. C., Collatz, G. J., Dolman, A. J. and DeFries, R. S.: Climate regulation of fire emissions and deforestation in equatorial Asia, Proc. Natl. Acad. Sci. U. S. A., 105(51), 20350–20355, doi:10.1073/pnas.0803375105, 2008.
Wolf, S., Keenan, T. F., Fisher, J. B., Baldocchi, D. D., Desai, A. R., Richardson, A. D., Scott, R. L., Law, B. E., Litvak, M. E., Brunsell, N. A., Peters, W. and Laan-Luijkx, I. T. van der: Warm spring reduced carbon cycle impact of the 2012 US summer drought, Proc. Natl. Acad. Sci., 113(21), 5880–5885, doi:10.1073/pnas.1519620113, 2016.
Wolter, K. and Timlin, M. S.: El Niño/Southern Oscillation behaviour since 1871 as diagnosed in an extended multivariate ENSO index (MEI.ext), Int. J. Climatol., 31(7), 1074–1087, doi:10.1002/joc.2336, 2011.
Wu, J., Albert, L. P., Lopes, A. P., Restrepo-Coupe, N., Hayek, M., Wiedemann, K. T., Guan, K., Stark, S. C., Christoffersen, B., Prohaska, N., Tavares, J. V., Marostica, S., Kobayashi, H., Ferreira, M. L., Campos, K. S., Silva, R. da, Brando, P. M., Dye, D. G., Huxman, T. E., Huete, A. R., Nelson, B. W. and Saleska, S. R.: Leaf development and demography explain photosynthetic seasonality in Amazon evergreen forests, Science, 351(6276), 972–976, doi:10.1126/science.aad5068, 2016.
Xu, L., Samanta, A., Costa, M. H., Ganguly, S., Nemani, R. R. and Myneni, R. B.: Widespread decline in greenness of Amazonian vegetation due to the 2010 drought, Geophys. Res. Lett., 38(7), L07402, doi:10.1029/2011GL046824, 2011.
Yin, Y., Ciais, P., Chevallier, F., van der Werf, G. R., Fanin, T., Broquet, G., Boesch, H., Cozic, A., Hauglustaine, D., Szopa, S. and Wang, Y.: Variability of fire carbon emissions in equatorial Asia and its nonlinear sensitivity to El Niño, Geophys. Res. Lett., 2016GL070971, doi:10.1002/2016GL070971, 2016.
Zhao, M. and Running, S. W.: Drought-Induced Reduction in Global Terrestrial Net Primary Production from 2000 Through 2009, Science, 329(5994), 940–943, doi:10.1126/science.1192666, 2010.
Zhou, L., Tucker, C. J., Kaufmann, R. K., Slayback, D., Shabanov, N. V. and Myneni, R. B.: Variations in northern vegetation activity inferred from satellite data of vegetation index during 1981 to 1999, J. Geophys. Res. Atmospheres, 106(D17), 20069–20083, doi:10.1029/2000JD000115, 2001.

Acknowledgements

C.Y. and P.C. acknowledge funding from the European Commission's 7th Framework Programme, under grant agreement number 603542 (LUC4C). The work of F.C. was funded by the Copernicus Atmosphere Monitoring Service, implemented by the European Centre for Medium-Range Weather Forecasts (ECMWF) on behalf of the European Commission. Taejin Park was supported by the NASA Earth and Space Science Fellowship Program (grant no. NNX16AO34H). We thank all the scientists involved in the surface and aircraft measurement of atmospheric CO_2 concentration and in archiving these data and making them available. We also thank Dr. Matthias Forkel and the anonymous reviewer for their review comments that helped improving the manuscript quality.

Author contributions

P.C., F.C., C.Y. and A.B. conceived the study. C.Y. performed the analysis and made the first draft. F.C. and C.R. provided the inversion data. T. P. provided the NDVI data. All authors contributed to the interpretation of the results and writing of the paper.

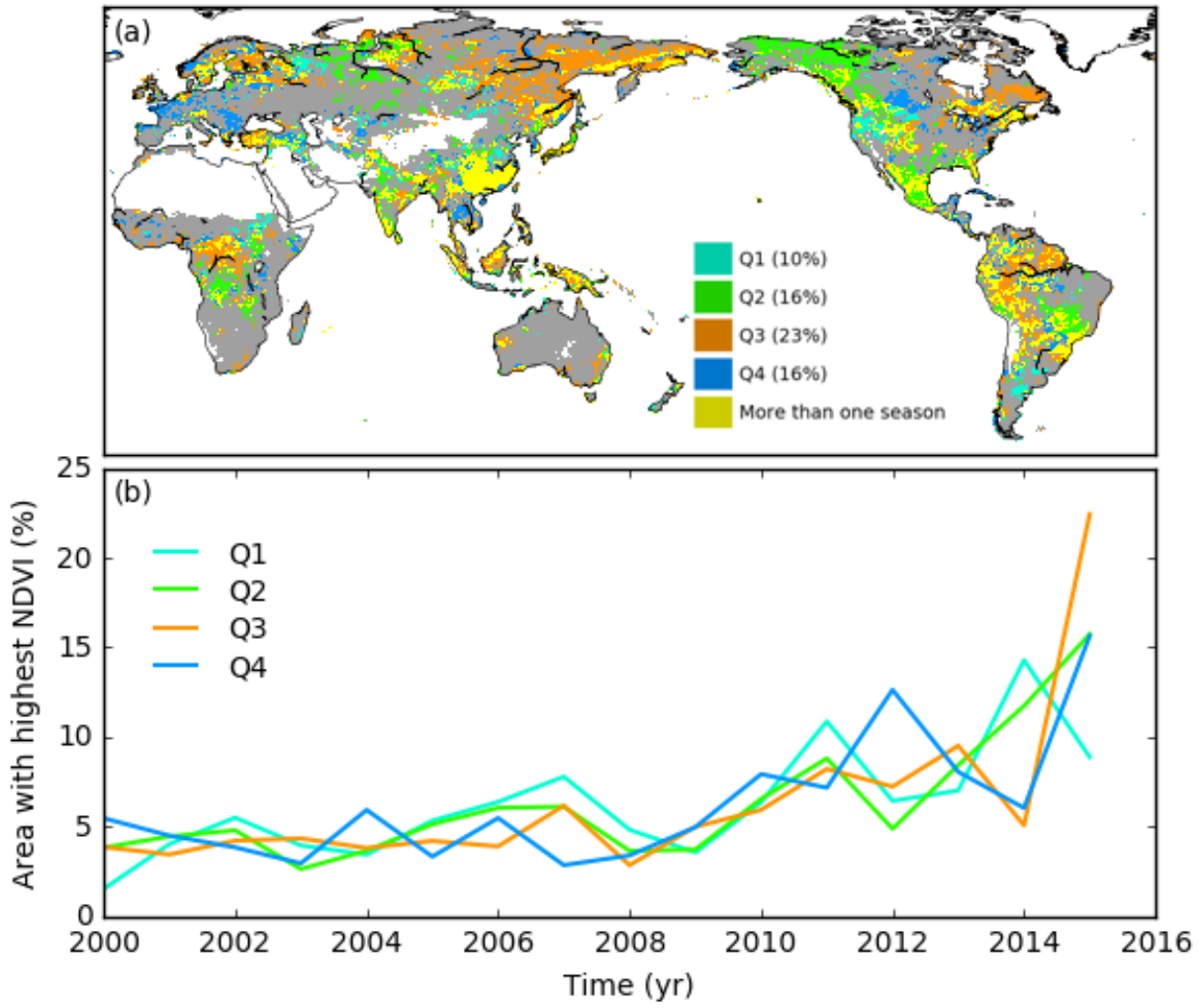

Figure 1 Year 2015 as the greenest year over the period 2000-2015. (a) Distribution of seasons for which 2015 NDVI ranks the highest during the period 2000-2015. Yellow-coloured pixels indicate grid cells where 2015 NDVI ranks highest for more than one season. For each season, the fraction of global vegetated land area for which 2015 NDVI ranks highest is shown in the inset colour bar. (b) Temporal evolution of the percentage of vegetated land with highest NDVI over 2000-2015 for each season and different years. The sum total of vertical-axis values for each season over all years is 100%. Q1 = January–March; Q2 = April–June; Q3 = July–September; Q4 = October–December.

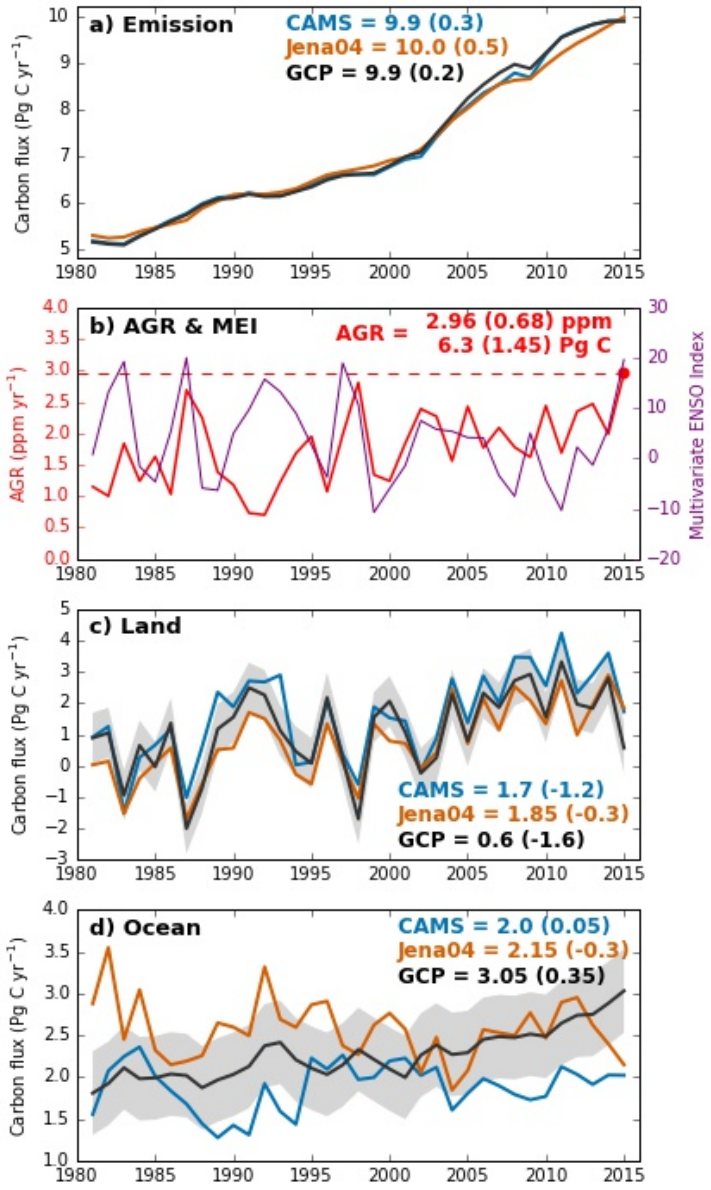

Figure 2 Global carbon fluxes and atmospheric CO_2 growth rates for 1981–2015. (a) Carbon emissions from fossil fuel and industry used in the CAMS (blue) and Jena04 (orange) inversions, (b) annual atmospheric CO_2 growth rate (AGR, in red) from NOAA/ESRL linked with Multivariate ENSO Index (in purple), and (c) land and (d) ocean carbon sinks for 1981-2015. Emissions and land and ocean carbon sinks from the Global Carbon Project (GCP, in black) are also shown for comparison. In subplots c and d, a carbon flux of 0.45 Pg C yr^{-1} was used to correct inversion-derived land and ocean sinks to account for pre-industrial land-to-ocean carbon flux as in Le Quéré et al. (2016). All numbers indicate values in 2015 (Pg C yr^{-1}, rounded to ±0.05 Pg C yr^{-1}), with those in brackets showing linearly de-trended anomalies for the same

year.

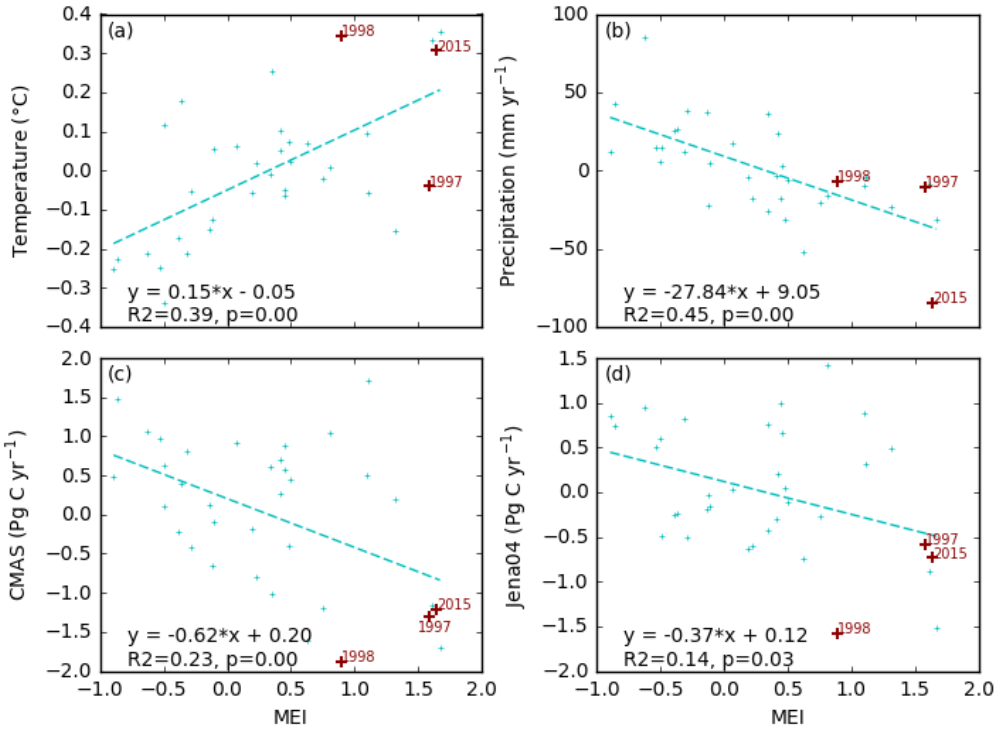

Figure 3 Relationships between anomalies of (a) land air temperature, (b) land precipitation, (c) land carbon fluxes by the CAMS inversion, (d) land carbon fluxes by the Jena04 inversion, and the Multivariate ENSO Index (MEI). All variables are linearly de-trended over 1981–2015.

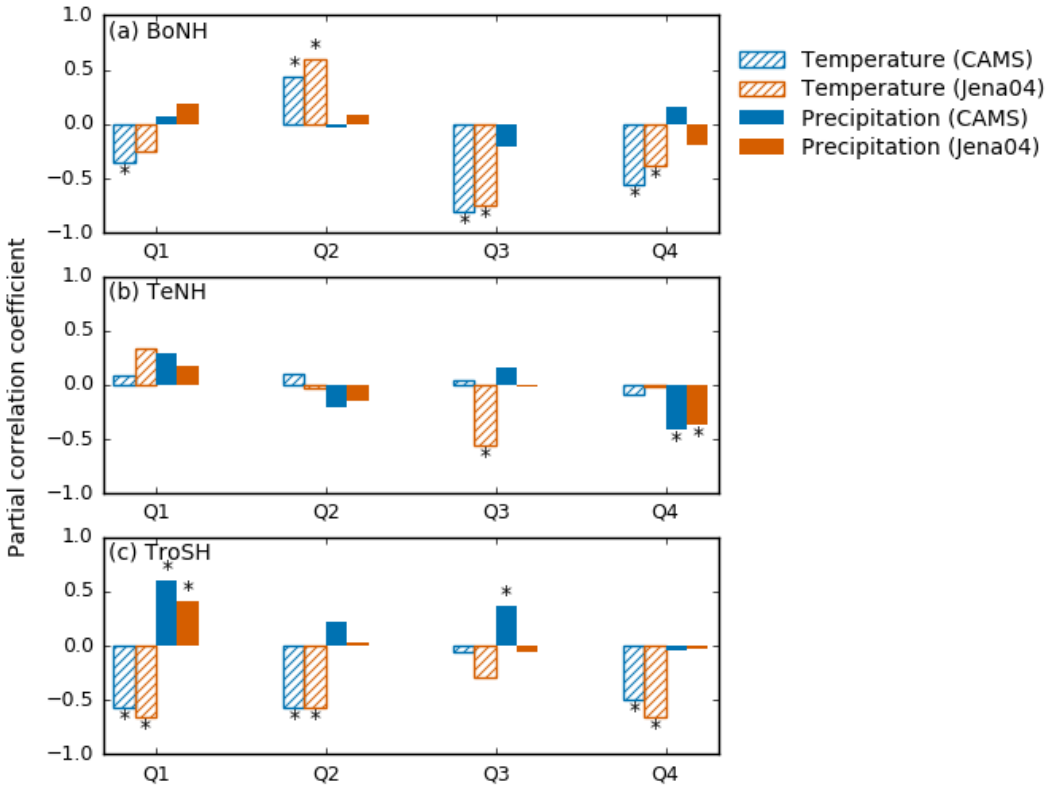

Figure 4 Partial correlation coefficients of de-trended annual anomalies of land carbon fluxes by CAMS and Jena04 inversions against the anomalies in temperature and precipitation of different seasons. n = 34. The asterisk indicates significant correlation ($p<0.05$).

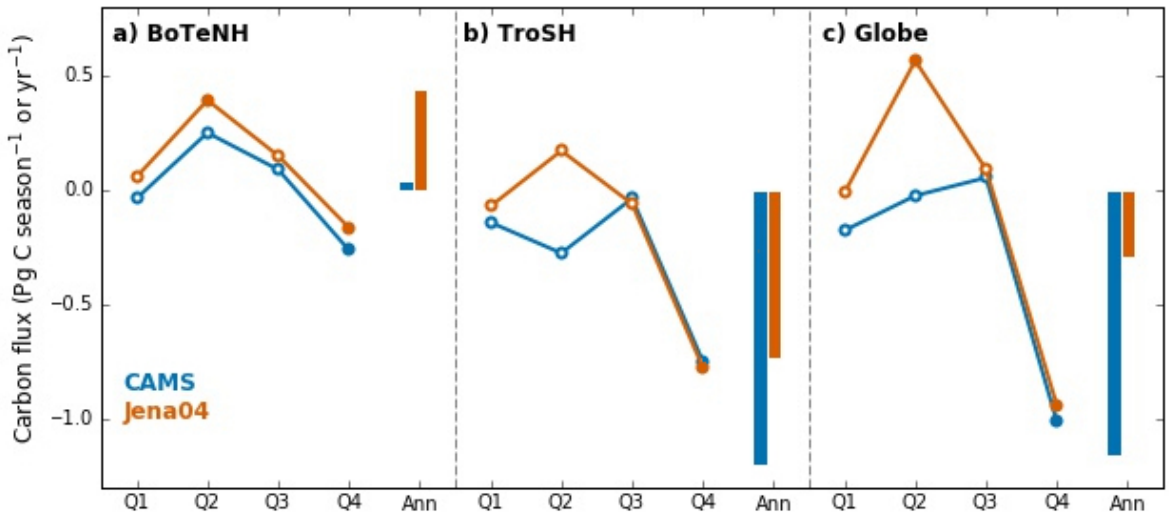

892

893 **Figure 5** Seasonal land carbon uptake anomalies in 2015. Data are linearly de-trended over
894 1981-2015 for different seasons in 2015, by CAMS (blue) and Jena04 (orange) inversion data.
895 Open or solid dots indicate seasonal values (Pg C seasaon^{-1}) and vertical bars indicate annual
896 sum (Pg C yr^{-1}). Data are shown for: (a) boreal and temperate Northern Hemisphere (BoTeNH, >
897 23.5°N), (b) tropics and southern extratropical hemisphere (TroSH, < 23.5°N) and (c) the whole
898 globe. Solid dots indicate seasonal land carbon uptake anomalies below 10th or above 90th
899 percentiles over 1981-2015.

900

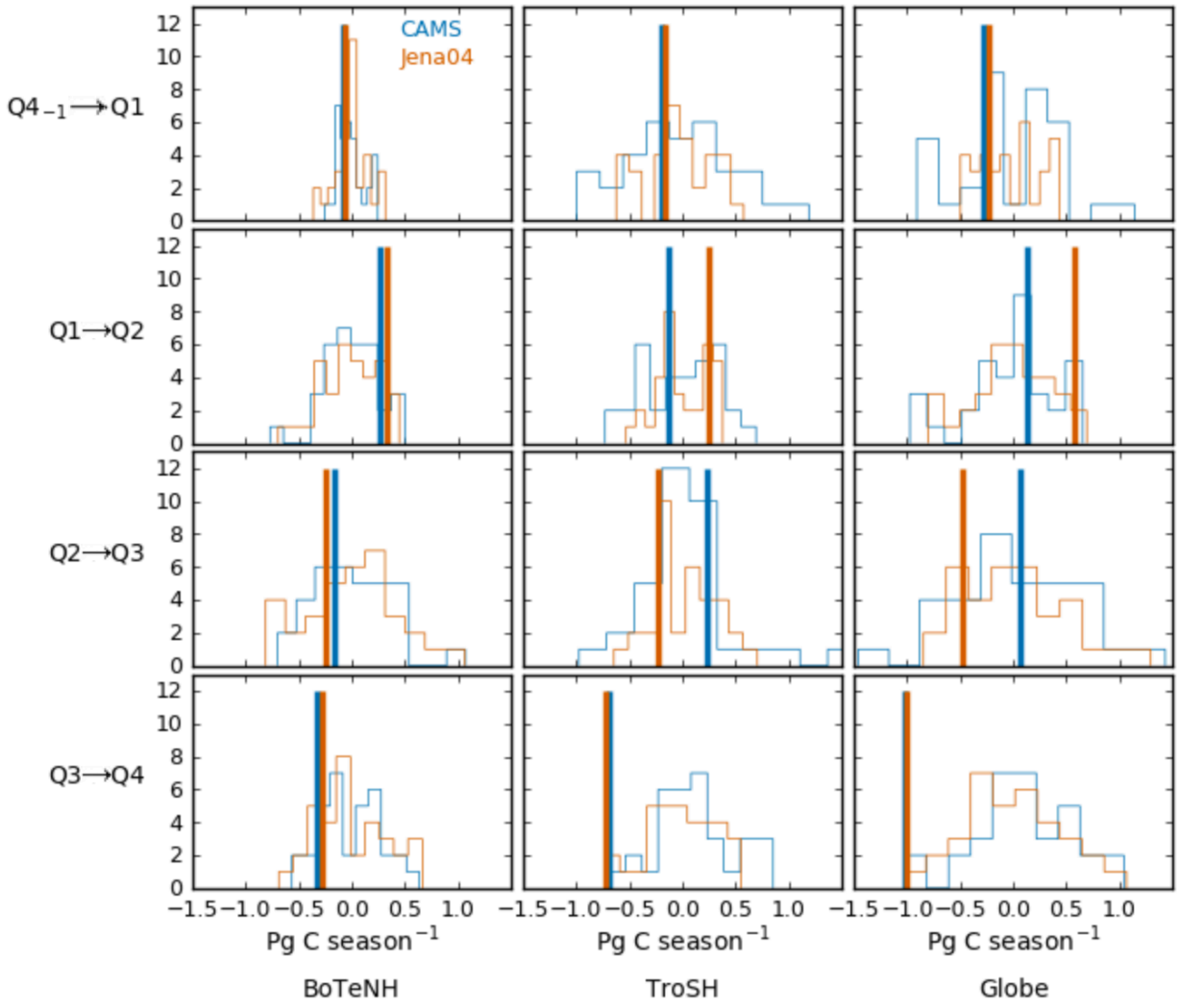

Figure 6 Extremeness of transitions in seasonal land carbon uptake anomaly in 2015. Lines of histograms for seasonal land carbon uptake transitions over 1981-2015 are shown for boreal and temperate Northern Hemisphere (BoTeNH, latitude > 23.5°N), tropics and extratropical Southern Hemisphere (TroSH, latitude < 23.5°N) and the whole globe. Transition between two consecutive seasons is defined as the linearly de-trended land carbon uptake anomaly in a given season minus that in the former one. X-axis shows the seasonal transitions in land carbon uptake anomalies (Pg C season^{-1}). Vertical orange solid lines indicate values for 2015.